On Practical Stability Regions for the Motion of a Small Particle close to the Equilateral Points of the Real Earth-Moon system[0]

Àngel Jorba
Departament de Matemàtica Aplicada i Anàlisi,
Universitat de Barcelona,
Gran Via 585, 08007 Barcelona, Spain
E-mail: angel@maia.ub.es

June 16, 1999

Abstract

This is a summary of a preliminary study on the existence of stability regions near the equilateral libration points of the real Earth–Moon system (here, by “real” Solar system we refer to the model defined by the ephemeris DE406 from JPL). We start from a model that takes into account the main effects coming from Earth, Moon and Sun to locate regions where trajectories are confined for long time intervals. Then, these regions are checked against a numerical integration that takes into account the real motion of Earth, Sun and the planets. This shows the existence of regions such that any initial condition inside them produces a trajectory that remains there for at least 1000 years.

1 Introduction

Let us start first with the simplest model for this problem, the well known Restricted Three Body Problem (from now on, RTBP). The RTBP models the motion of a particle under the gravitational attraction of the Earth and Moon (also called primaries), under the following assumptions: i) the particle is so small that it does not affect the motion of Earth and Moon; and ii) Earth and Moon are point masses that revolve in circular orbits around their common centre of mass. It is usual to take a rotating frame with the origin at the centre of mass, and such that Earth and Moon are fixed on the X axis, the (X, Y) plane is the plane of motion of the primaries, and the Z is orthogonal to the (X, Y) plane.

[0]This is the text of a talk delivered at the *III International Symposium HAMSYS-98. Geometrical Methods in Hamiltonian Systems and Celestial Mechanics* held in Pátzcuaro (México), December 7–11, 1998.

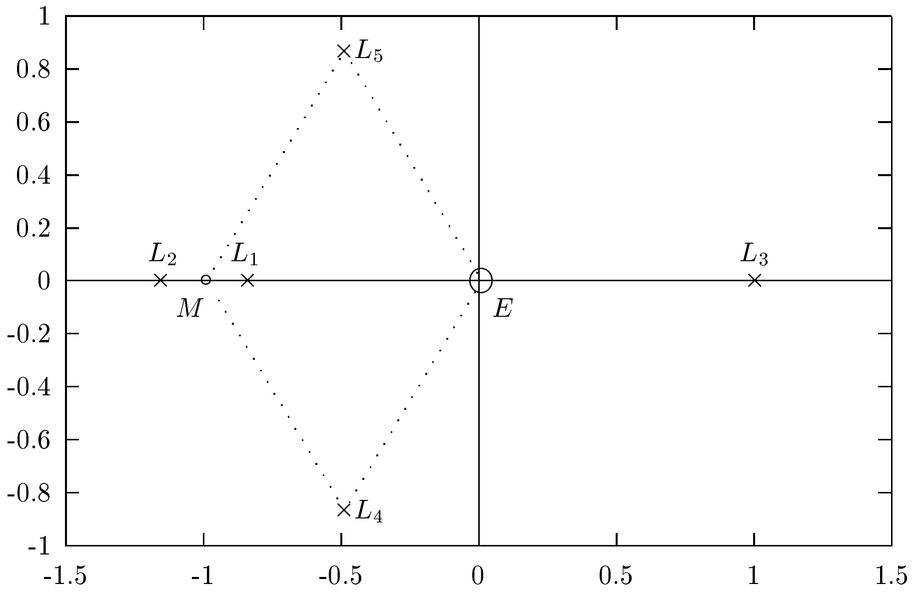

Figure 1: The five equilibrium points of the RTBP.

The units of distance, mass and time are defined such that the Earth–Moon distance, the total mass of the system (Earth+Moon) and the gravitational constant are all one. With these units, the period of the motion of Earth and Moon around the origin equals 2π. Defining momenta as $p_x = \dot{x} - y$, $p_y = \dot{y} + x$ and $p_z = \dot{z}$, the equations for the motion of the particle can be written as an autonomous three degrees of freedom Hamiltonian system. The corresponding Hamiltonian function is

$$H_{RTBP} = \frac{1}{2}(p_x^2 + p_y^2 + p_z^2) + yp_x - xp_y - \frac{1-\mu}{r_{PE}} - \frac{\mu}{r_{PM}}, \tag{1}$$

being $r_{PE}^2 = (x-\mu)^2 + y^2 + z^2$ and $r_{PM}^2 = (x-\mu+1)^2 + y^2 + z^2$.

It is well known that this Hamiltonian has five equilibrium points, that are displayed in Figure 1: three of them lay on the X axis (they are called collinear points, Eulerian points, or simply $L_{1,2,3}$), and the other two form an equilateral triangle (in the (X,Y) plane) with Earth and Moon (they are called triangular points, Lagrangian points or simply $L_{4,5}$). For more details see, for instance, [1] or [2]. It is also well known that, for the value of the masses of Earth and Moon, the triangular points are linearly stable. It is known that, under very general conditions, there exists a neighbourhood of these points such that any initial condition inside this neighbourhood produces a trajectory that remains close to the point for huge intervals of time (see [3], [4], [5], [6] and references therein).

On the other hand, let us consider the motion of a particle in the real Solar system, close to the triangular points of Earth and Moon. Here, by real system we refer to the one obtained from the well known JPL ephemeris [7]: the ephemeris contain the position of the main bodies of the Solar system (Earth, Moon, Sun and planets) so we can easily write the vector field acting on the particle. This is a numerically defined vector field, that we can integrate for the time span for which the ephemeris are available. Note that, for the real system, the triangular points are not longer equilibrium points since the hypotheses used to derive the RTBP are not satisfied. It is know that arbitrary trajectories starting near the (geometrically defined) triangular points go away after a short time (see [8] and references therein) and hence, the RTBP is not a good model to study this problem because it displays a quite different qualitative behavior.

In this talk we will first use the so called Bicircular Problem (from now on, BCP). This model can be seen as a time dependent periodic perturbation of the RTBP, that includes the main effect coming from the Sun. As far as we know, this model is first introduced in [1]. As we will see, the BCP model has some of the main features of the real model (for instance, the neighbourhood of the equilateral points is unstable).

Our purpose is to use the BCP model to describe some properties of the real model. In particular, we will compute, for the BCP, families of 2-D invariant tori near the equilateral points, as well as their normal behaviour. We will show (by computing the normal modes of the tori) that some of them are hyperbolic, while some others are elliptic. Those elliptic tori are found at some distance from the equilateral points. It is known that lower-dimensional normally elliptic tori give rise, under suitable hypotheses, to regions of effective stability around them (see [9], [10]). Finally, we will show, by means of numerical simulations, that some of these stability regions found in the BCP model subsist in the real system, at least for time spans of 1000 years.

This talk is based on results contained in [11], [12] and [13]. They can be downloaded from the web server `http:\\www.maia.ub.es/dsg`, in the `preprints` section.

2 The Bicircular Problem

Let us assume that Earth and Moon are point masses that revolve in circular orbits around their common centre of mass (as in the RTBP), and let us also assume that this centre of mass revolves in a circular orbit around the Sun (that is also considered as a point mass) that is fixed at the origin. We are also assuming that the motion of the three bodies is coplanar. The purpose of the Bicircular Problem is the study of the motion of an infinitesimal particle under the attraction of these three bodies. It is usual to take the same reference frame and normalized units as in the RTBP. So, in this system of reference, Earth and Moon are fixed on the x axis while the Sun is turning around the origin. Defining momenta as $p_x = \dot{x} - y$, $p_y = \dot{y} + x$ and $p_z = \dot{z}$, then the motion of the infinitesimal particle can be described by a Hamiltonian system that depends on time in a periodic way:

$$
\begin{aligned}
H_{BCP} &= \frac{1}{2}\left(p_x^2 + p_y^2 + p_z^2\right) + y p_x - x p_y - \\
&\quad -\frac{1-\mu}{r_{PE}} - \frac{\mu}{r_{PM}} - \frac{m_S}{r_{PS}} - \frac{m_S}{a_S^2}\left(y \sin\theta - x\cos\theta\right), \qquad (2)
\end{aligned}
$$

where $r_{PE}^2 = (x-\mu)^2 + y^2 + z^2$, $r_{PM}^2 = (x-\mu+1)^2 + y^2 + z^2$, $r_{PS}^2 = (x-x_S)^2 + (y-y_S)^2 + z^2$, $x_S = a_S\cos\theta$, $y_S = -a_S\sin\theta$, and $\theta = \omega_S t$. The values used for these constants are

μ	$=$	0.012150581623433623	m_S	$=$	328900.54999999906
ω_S	$=$	0.925195985518289646	a_S	$=$	388.81114302335106

Table 1: Floating point values used for the different constants of the BCP. Not all the digits are significative (they appear because the definition of these quantities involves quotients).

listed in Table 1. We stress that the BCP can be written as a periodic time dependent perturbation of the RTBP:

$$H^{\varepsilon}_{BCP} = H_{RTBP} + \varepsilon \widehat{H}_{BCP}, \quad \widehat{H}_{BCP} = -m_S \left(\frac{1}{r_{PS}} + \frac{y \sin\theta - x \cos\theta}{a_S^2} \right), \tag{3}$$

and it is clear that $H^{\varepsilon=0}_{BCP} = H_{RTBP}$, and that $H^{\varepsilon=1}_{BCP} = H_{BCP}$.

Now, let us focus on the L_5 point (due to the symmetries of the RTBP and the BCP, the same results will be valid for L_4; of course, this is not true for the real system). As the vector field of the perturbation $\varepsilon \widehat{H}_{BCP}$ does not vanish on L_5, this point is not longer an equilibrium solution. An straightforward application of the Implicit Function Theorem shows that, under a generic non-resonance condition (satisfied in this case) and assuming ε small enough, L_5 is replaced by a periodic orbit with the same period as the perturbation. This orbit tends to L_5 when ε tends to zero.

Let us consider now the Poincaré section defined by $t = 0 \bmod T_S$, where $T_S = 2\pi/\omega_S$ is the period of the perturbation. Let us call P_ε the corresponding Poincaré map. Note that the fixed points of this map correspond to periodic orbits (of period T_S) for the flow, and vice versa.

Now, by means of a continuation process, let us compute the fixed points of P_ε for ε ranging between 0 and 1. The results are displayed in Figure 2 (left), where the horizontal axis shows the x coordinate of the fixed point and the y coordinate refers to the value of ε. Note that, for $\varepsilon = 1$, there are three fixed points of P_ε that are close to L_5. The (x, y) projection of the corresponding periodic orbits for the flow are displayed in Figure 2 (right).

By computing the eigenvalues of the differential of P_ε at the fixed points, one can see that orbit PO1 is unstable, and that orbits PO2 and PO3 are linearly stable (see Figure 2). Moreover, the three periodic orbits have an elliptical mode very close to the (z, p_z) plane. In what follows, we will refer to this mode as the vertical mode of the corresponding periodic orbit. For more details about the BCP, see, for instance, [14] or [15].

2.1 The vertical families of 2-D tori of the BCP

Let us now consider the vertical mode of one of the periodic orbits. It is known that, under generic conditions (see [9], [10]), there exists a Cantor family of 2-D invariant tori that extend this linear mode into the complete (i.e., nonlinear) system. This is very similar

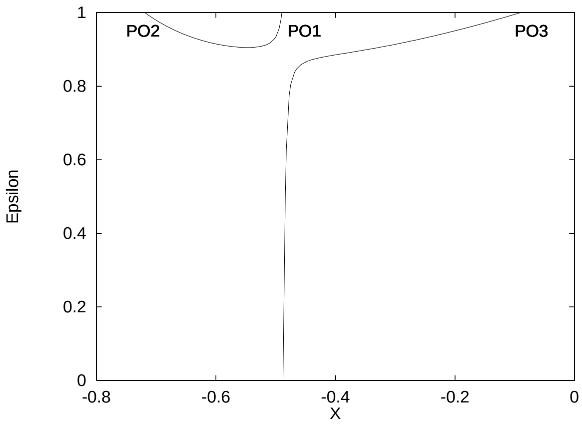

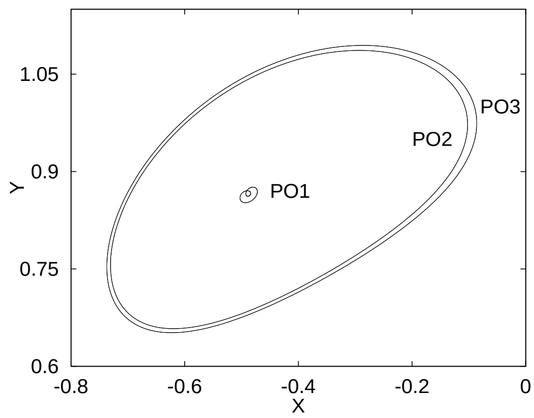

Figure 2: Left: Continuation of the periodic orbit that replaces L_5 in the BCP. Right: The three periodic orbits that appear in the left plot for $\varepsilon = 1$.

to the well-known Lyapunov centre theorem: instead of obtaining a (smooth) family of periodic orbits, one obtains a (Cantor) family of 2-D tori.

Next, we will focus on the computation of these vertical families of two-dimensional tori. Their interest will be clear later on.

3 Computation of invariant curves

In this section we will briefly explain a numerical method for computing families of invariant curves of high dimensional maps. The method does not require the knowledge of an algebraic expression for the map, it only requires a procedure to numerically evaluate the map (and its differential) at a given point. So, it is a suitable method to be applied to the Poincaré map of an ODE. More details can be found in [11].

3.1 A Newton method

Let us consider a map f from an open set of $\mathbb{R}^n$ into itself, with an invariant curve with (irrational) rotation number ω; this is, we assume that there exist a map $x : \mathbb{T}^1 \to \mathbb{R}^n$ such that

$$f(x(\theta)) = x(\theta + \omega), \qquad \text{for all } \theta \in \mathbb{T}^1. \tag{4}$$

To simplify the discussion, let us assume that we know the value ω, so we only need to determine the Fourier coefficients of the function $x(\theta)$,

$$x(\theta) = a_0 + \sum_{k>0} a_k \cos(k\theta) + b_k \sin(k\theta), \quad k \in \mathbb{N}.$$

Let us now fix a truncation value N (the selection of N will be discussed in Section 3.3), and let us try to compute an approximation to the $2N + 1$ unknown coefficients a_0, a_k and b_k, $0 < k \le N$. First, let us define a mesh of $2N + 1$ points on $\mathbb{T}^1$,

$$\theta_j = \frac{2\pi j}{2N+1}, \quad 0 \le j \le 2N.$$

Imposing condition (4) on the points of this mesh we obtain the system of $2N+1$ equations,

$$f(x(\theta_j)) - x(\theta_j + \omega) = 0, \quad 0 \le j \le 2N, \tag{5}$$

that we will solve, by means of the Newton method, to determine the $2N + 1$ unknown Fourier coefficients.

The differential of this equation can be easily obtained by using the chain rule: Let F be the function that maps each sequence of $2N+1$ Fourier coefficients $(a_0, a_1, b_1, a_2, b_2, \ldots, a_N, b_N)$ on the vector of $2N + 1$ components given by

$$\left(f(x(\theta_j)) - x(\theta_j + \omega)\right)_{0\le j\le 2N}.$$

Hence, denoting by $Df(p)$ the Jacobian of f at a given point $p \in \mathbb{R}^n$, we have

$$\frac{\partial F}{\partial a_k} = Df(x(\theta_j))\frac{\partial x(\theta)}{\partial a_k}(\theta_j) - \frac{\partial x(\theta + \omega)}{\partial a_k}(\theta_j).$$

Note that $Df(x(\theta_j))$ can be easily computed, and that

$$\frac{\partial x(\theta)}{\partial a_k}(\theta_j) = I_n \cos(k\theta_j), \qquad \frac{\partial x(\theta + \omega)}{\partial a_k}(\theta_j) = I_n \cos(k\theta_j + k\omega), \tag{6}$$

where I_n denotes the $n \times n$ identity matrix. Similar formulas hold for the derivatives with respect to b_k. From these formulas one can easily assemble the Jacobian matrix of F: it consist of $(2N + 1) \times (2N + 1)$ boxes, being each box a $n \times n$ matrix (we recall that a_k and b_k are arrays of n components).

3.2 On the uniqueness

If $x(\theta)$ denotes a Fourier series corresponding to an invariant curve then, for any $\varphi \in \mathbb{T}^1$, $y(\theta) \equiv x(\theta+\varphi)$ is a different Fourier series (i.e., the Fourier coefficients are different) that represents the same invariant curve as $x(\theta)$. This lack of uniqueness in the representation of the invariant curve implies that the differential of the function F around an invariant curve will have a one-dimensional kernel. To deal with this situation, we will add an extra condition imposing that one of the components of $x(\theta)$ has a prescribed value when θ is zero. In our case we will use the condition $z = 0$ because, as we will see, all the invariant curves cross transversally the surface $z = 0$. As this is a linear condition, it is trivial to add the corresponding row in the differential. Note that now we have to solve a linear system that has a unique solution, but it is not squared: it has an "extra" equation. We will use standard Gaussian elimination with row pivoting. The pivoting strategy will take care of sending to the last row the equation that is linearly dependent of the other equations. So, after the triangularisation process and except by rounding errors, the last equation should read like "$0 = 0$". Hence, we can simply skip this equation and solve the triangular system in the usual way.

3.3 Error estimation

To select the truncation value N used in the discretization (see Section 3.1), we will use the following estimation for the error:

$$E(x,\omega) = \sup_{\theta\in\mathbb{T}^1} |f(x(\theta)) - x(\theta+\omega)|.$$

Clearly, x is an invariant curve with rotation number ω iff $E(x,\omega)$ is zero.

For each curve, we have estimated the quantity $E(x,\omega)$ by simply tabulating its value on a mesh of points on $\mathbb{T}^1$. Of course, this mesh must be finer (typically, we have used a 100 times finer mesh) than the one used to obtain (5) from (4). When this estimate is bigger than a prescribed threshold (here we have used 10^{-12}), the program automatically increases the number of Fourier coefficients and the number of discretizing points (i.e., it increases the truncation value N) and recomputes the invariant curve. This process is repeated until the estimated error $E(x,\omega)$ is lower than 10^{-12}.

3.4 Results

By means of a standard continuation procedure (see details in [11]), we have computed the vertical families of 2-D tori for the three periodic orbits PO1, PO2 and PO3, for several values of ε (see Figure 3). For definiteness, let us call Fj the family that is born in POj, $j = 1,2,3$. Note that the families F1 and F2 are connected, as it is suggested by the diagram in Figure 2 (left).

As PO1 is hyperbolic, we expect that the tori in F1 are also hyperbolic, at least for moderate values of the vertical amplitude. PO2 and PO3 are elliptic orbits so, under generic conditions, it is expected that most of the tori in families F2 and F3 with a small vertical amplitude are also normally elliptic.[1] The study of the normal stability of these families is the topic of Section 5.

4 Stability regions

It is also known that, under generic conditions of analyticity, non-degeneracy and non-resonance, a lower dimensional and normally elliptic invariant tori is surrounded by a region of effective stability. Here, by "region of effective stability" we mean that trajectories starting inside this region need a extremely long time to escape of a neighbourhood of the torus [10].

Here we will try to estimate this region by means of purely numerical methods (see [16] for a semi-analytical approach in the case of a periodic orbit). So, given a 2-D torus on one of these families, we will first select the unique point a_0 on it satisfying $t = 0$ (i.e., we are selecting the point on the Poincaré section), $z = 0$ and $\dot z = \dot z_0 > 0$ ($\dot z_0$ will be used as a parameter). Then, we will take a 2-D mesh of points around the (x,y) coordinates of a_0 (and inside the (x,y) plane), keeping fixed all the remaining coordinates.

[1] Although most of them are going to be elliptic tori, a small measure set of them is expected to be normally hyperbolic, due to some resonances involving internal and normal frequencies.

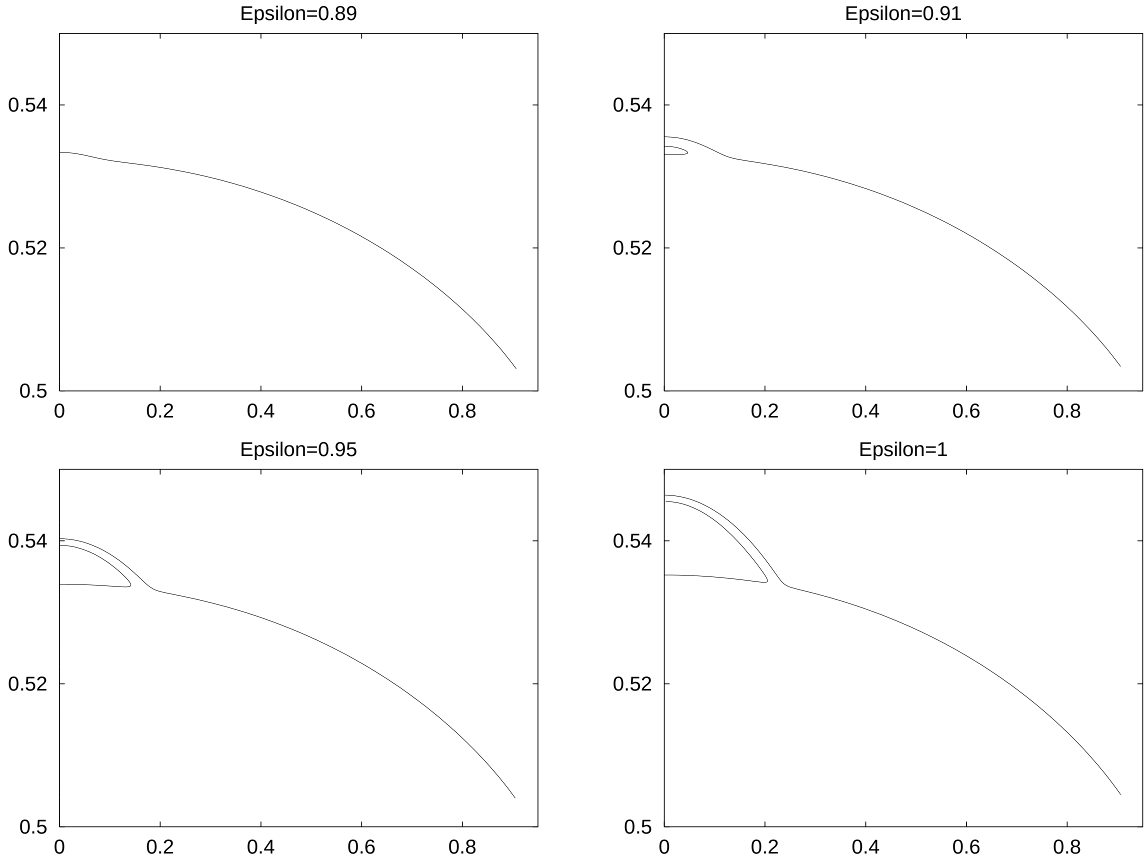

Figure 3: Vertical families of invariant tori for several values of ε. The horizontal axis shows the value of the coordinate $\dot{z}$ of the invariant curve when $z = 0$, and the vertical axis shows the corresponding rotation number. The gaps that conform the Cantor structure are too narrow to be seen at this scale.

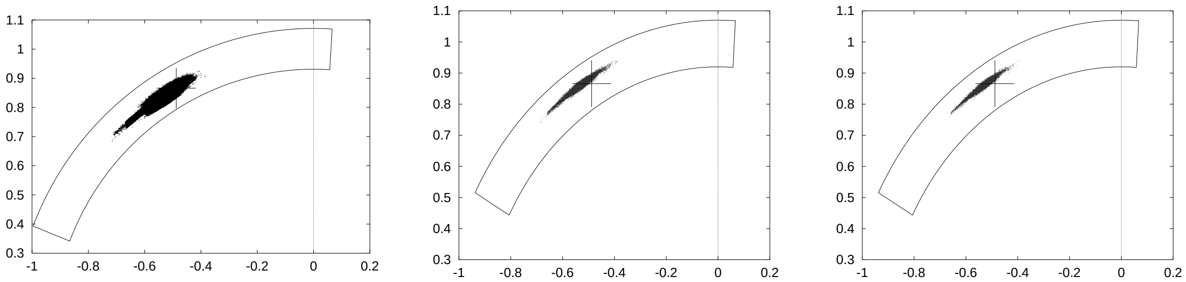

Figure 4: Left: stability region for the BCP, for $\dot{z} = 0.58$. Centre: stability region for the real model (500 years). Right: stability region for the real model (1000 years). The box corresponds to the explored region. The position of L_5 is marked with a big "+" sign.

Then, we will use each point on the mesh as initial condition for a numerical integration of the vector field. If the trajectory does not cross the $y = -0.5$ plane, and it does not approach collision with Earth and Moon during the integration time (see Section 4.1), we admit that the initial condition belongs to the stability region.

Next, in Section 4.1, we will summarize the results from the simulations for the BCP and for the real system.

4.1 Some numerical simulations

Let us first select the 2-D torus of the family F3 such that, in the Poincaré section $t = 0$, z is zero and $\dot{z}$ is 0.58 (the reasons for this selection will be clear later). Let us first make a numerical simulation around this torus, as explained above. Figure 4 (left) displays the set of initial conditions (x, y) such that the corresponding trajectory does not escape for a time span of 5000 periods of the Moon. Then, let us take this mesh to make a numerical simulation for the real system, by using the JPL ephemeris (file DE406). Here, the initial integration time is the first full Moon of year 2000 (this is to have a relative position of Earth, Moon and Sun similar to the one of the BCP when $t = 0$). Figure 4 (centre) shows the initial conditions that do not escape after 500 years, and Figure 4 (right) contains the ones that do not escape after 1000 years. The unit of distance in the scales of the plots is the Earth-Moon distance. Note that the size of these regions is quite big.

Let us now consider the torus (of the family F3) corresponding to $z = 0$ and $\dot{z} = 0.83$. Doing the same simulations as before, one obtains the results displayed in Figure 5. As before, the left graphic refers to the BCP (the integration time is again 5000 revolutions of the Moon), and the centre and right graphics refer to the real system (for 500 and 1000 years respectively). This kind of stability was already observed in [14], but with smaller regions and much shorter time intervals (around 60 years). The main improvements in this work come from the computation of the vertical families of 2-D tori for the BCP and to use initial conditions around them.

A natural question is whether this is the typical behaviour around the vertical family. To this end, we have repeated the above simulations around several tori in family F3. The results are summarized in Figure 6 (more complete results and explanations can be found in [12]). The horizontal axis refers to the $\dot{z}$ coordinate of the torus in the Poincaré section,

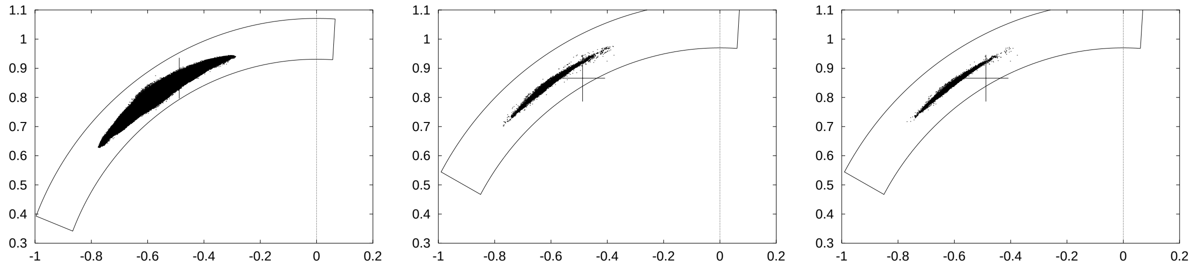

Figure 5: As Figure 4, but for the case $\dot{z} = 0.83$.

and the vertical axis contains the number of points of the initial mesh that do not escape for 1000 years (as the meshes used have the same density, the number of surviving points can be considered an estimate of the size of the stable region). Apparently, the stability region has two big components, centered (approximately) around the values $\dot{z} = 0.58$ and $\dot{z} = 0.83$.

Simulations for longer time intervals on the BCP model (as well as a discussion on the relevance of the total simulation time) can be found in [15] and [12]. For longer simulations on the JPL model, see [12].

5 Normal behaviour of lower dimensional tori

Note that the numerical simulation is not a good method to detect if a given object is normally stable. For instance, an hyperbolic object can have almost coincident stable and unstable manifolds (i.e., with a very small splitting), such that the trajectories look like confined in a neighbourhood of moderate size (in fact, they keep escaping and coming back). To detect this situation, it is very convenient to have methods to compute the normal behaviour of invariant tori. Note that the linear approximation to the normal behaviour of a torus is given by a linear differential equation that depends on time in a quasi-periodic way.

The study of linear systems that depend on time in a quasi-periodic way is an old topic of the theory of ODE. Here we will focus on the numerical computation of the normal behaviour of these systems. This problem has been addressed in [17] and [18] (see also references therein). Here we will explain a method for numerically compute the normal modes of an invariant curve. This method can also be applied to tori of higher dimensions (see [13] for the details).

Let $x(\theta)$ be an invariant curve of a n-dimensional map f, and let ω be the corresponding rotation number. Hence, they satisfy equation (4). Then, it is not difficult to see that the linear behaviour around this invariant curve is given by the dynamical system

$$\left.\begin{array}{rcl} x_{i+1} & = & A(\theta_i)x_i, \\ \theta_{i+1} & = & \theta_i + \omega, \end{array}\right\} \tag{7}$$

where $x_i \in \mathbb{R}^n$. To keep the notation simple, we have used again the letter x to denote an infinitesimal displacement w.r.t. the invariant curve.

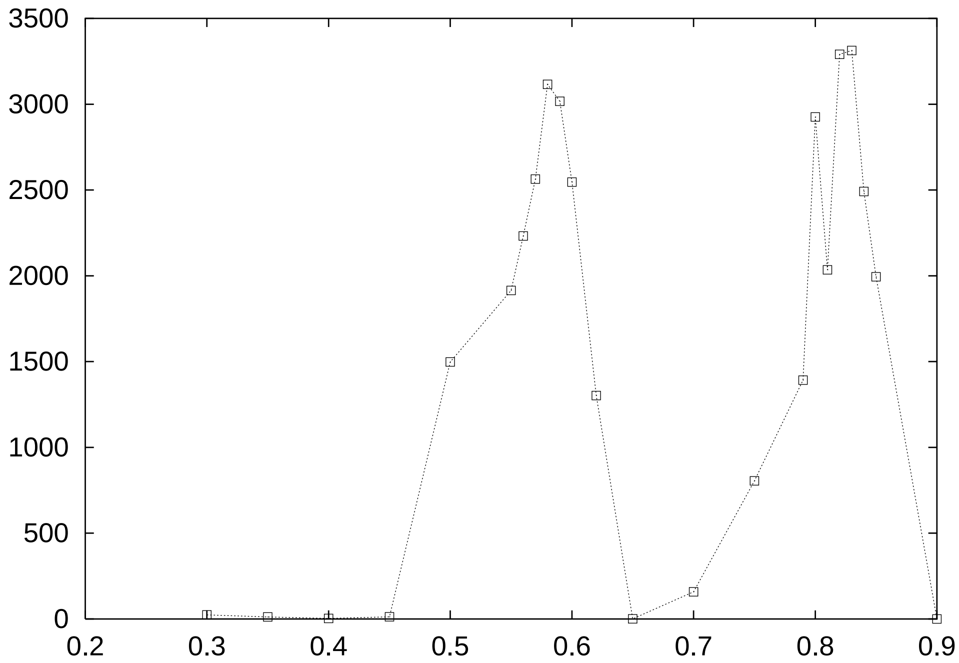

Figure 6: Horizontal axis: value of the $\dot{z}$ coordinate. Vertical axis: an estimate of the size of the stability region (see text).

5.1 On the reducibility of linear quasi-periodic systems

The system (7) is said to be reducible if there exists a linear change of variables, $x_i = C(\theta_i)y_i$, such that the transformed system,

$$\left.\begin{array}{rcl} y_{i+1} & = & B(\theta_i)y_i, \\ \theta_{i+1} & = & \theta_i + \omega, \end{array}\right\} \qquad B(\theta) = C^{-1}(\theta+\omega)A(\theta)C(\theta),$$

satisfies that the matrix B does not depend on the angles θ, i.e., that the matrix B is constant. Note that the normal behaviour of a reducible system like (7) is completely determined by the eigenvalues of the reduced matrix B.

It is known that not all the linear quasi-periodic systems like (7) are reducible, but is also known that reducibility appears in many cases. In the concrete case of elliptic lower dimensional tori of Hamiltonian systems, it turns out that the usual proofs of existence produce reducible tori. Hence, the possible non-reducibility must be confined into a set of very small measure. As far as we know, the only paper that proves the existence of lower dimensional tori without using reducibility conditions is [19], although it does not show the existence of non-reducible tori.

Let us start by considering reducible linear systems like (7). This is, we are assuming that there exists a matrix $C(\theta)$, $\theta \in \mathbb{T}^1$, such that the matrix $B = C^{-1}(\theta+\omega)A(\theta)C(\theta)$ does not depend on θ. Let $\mathcal{V}$ be the vector space $\{\psi : \mathbb{T}^1 \mapsto \mathbb{R}^n\}$, and let us define the translation $\mathcal{T}_\omega$ as $\mathcal{T}_\omega x(\theta) = x(\theta+\omega)$. Let us consider the following generalized eigenvalue problem: to look for couples $(\lambda, \psi) \in \mathbb{C} \times \mathcal{V}$ such that

$$A(\theta)\psi(\theta) = \lambda \mathcal{T}_\omega \psi(\theta). \tag{8}$$

It is not difficult to show that (see [13] for more details):

1. If λ is an eigenvalue of B, then λ is an eigenvalue of (8).

2. If λ is an eigenvalue of (8), then there exists $k \in \mathbb{Z}$ such that $\lambda \exp(\sqrt{-1}\,k\omega)$ is an eigenvalue of B.

The numerical method we will use to compute the normal behavior of the invariant curves is based on computing the spectrum of a discretization of (8), as explained in Section 5.2.

It is interesting to note that the reducibility hypothesis introduces strong restrictions on the spectrum of (8). Hence, it seems possible to detect non-reducibility by computing the spectrum of a discretized version of (8) and showing that it is not compatible with the reducibility condition (see [13]). It is also worth noting that all the examples included in this paper have a discretized spectrum compatible with reducibility.

5.2 Methodology

The numerical method for computing the normal behaviour of the invariant curves is then the following: once the invariant curve has been obtained (by means of the Newton method explained in Section 3), we can easily obtain the matrix corresponding to the discretization of the operator that maps $\psi(\theta)$ to $A(\theta)\psi(\theta)$: note that this matrix is precisely the first term that appear in the differential of F in (6), $Df \cdot \frac{\partial x}{\partial a_k}$, but composed with the linear operator that, given a set of points, produces the Fourier coefficients. Let us denote this first part of the differential by $\mathcal{A}$. Then, the initial eigenvalue problem is equivalent to the (standard) eigenvalue problem

$$\mathcal{T}_{-\omega}\mathcal{A}\psi = \lambda\psi. \tag{9}$$

Note that, as the matrix of $\mathcal{T}_{-\omega}$ is block diagonal (in the usual basis of sinus and cosinus, these blocks are 2×2) and very easy to write, we obtain the discretized matrix of $\mathcal{T}_{-\omega}\mathcal{A}$ by simply multiplying the matrices of these two discretizations. Then, it is not difficult to obtain the corresponding eigenvalues.

Once these eigenvalues have been obtained, the next problem is to classify them. We recall that, if the initial system is reducible, these eigenvalues can be expressed in the form $\exp(\sqrt{-1}\,k\omega)\lambda$, where λ is an eigenvalue of the reduced matrix. Note that ω is known here, and we are only interested in identifying the values λ (note that, in the elliptic case, these values are not uniquely defined, see [13]).

5.3 Some results

Figure 7 displays, in the complex plane, the eigenvalues of (7) for some tori in the families F1 and F2. More concretely, we display the transition from F1 to F2 (see also the bottom-right plot in Figure 3). In the left plot, we observe three circles, two of them correspond to hyperbolic behaviour (those are the ones of radius different from 1), while the circle of radius 1 correspond to neutral and elliptic behaviour. Looking at the (numerical values of) the eigenvalues of modulus one, it is easily observed that there are only two of them that are real: 0.915799019153 and 1.091942641438, while all the others can be found as a rotation (of an angle multiple of ω) of them. In the set of eigenvalues of modulus 1, one finds a couple of eigenvalues equal to one (they come from the symplectic structure of this problem), their rotations by a multiple of ω, the normal frequencies and their corresponding rotations. They are studied with more detail in [13]. The sequence of the three plots in Figure 7 shows how the change of stability takes place. The study of the bifurcations that appear here is left for a future work.

Figure 8 (left) shows the eigenvalues for a torus in the family F3. In the right plot, we display the modulus of the eigenvalues against an index labelling them. It is clearly seen the mild instability of this torus. In this case, there are no eigenvalues of modulus different than one that are real. This corresponds to a complex saddle, where the modulus of the eigenvalues of the saddle are 0.999897464349 and 1.000102546166.

Due to the errors introduced in the truncation of the linear operator (9), we expect that high order modes will have a rather big error. Those modes are easily detected since there are no other eigenvalues obtained from them by rotations of angle $k\omega$. Moreover, they do not persist if the truncation order of the operator is increased.

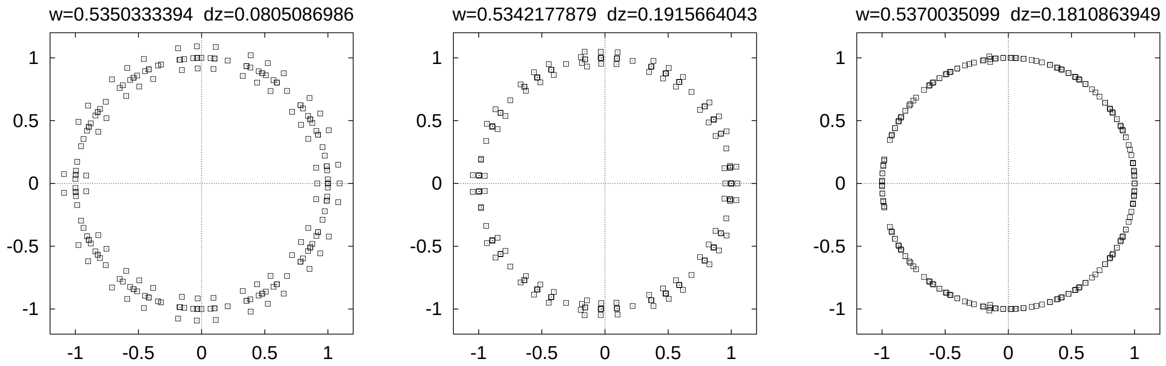

Figure 7: Eigenvalues in the transition from family F1 to F2. The corresponding rotation number (`w`) and the value of $\dot{z}$ (`dz`) are included at the top of each plot.

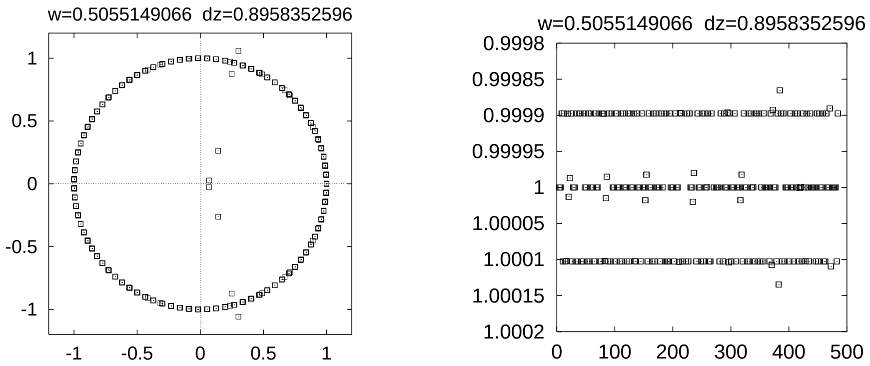

Figure 8: A mild instability in family F3.

6 Conclusions

The main purpose of this work has been to show the existence of regions of practical stability close to the equilateral points of the real Earth-Moon system. We have focused the discussion on the L_5 point, and similar results hold for L_4 ([12]). Although this result is based on a numerical integration of the real system, it has been shown how some standard techniques from dynamical systems theory allow to guess, approximately, where these regions should be. So, the final numerical exploration has only been done in a small part of phase space.

An interesting point is the persistence of these regions for longer time intervals because, in this case, they could contain some kind of dust or even some asteroids. Note that an asteroid inside this region must oscillate up and down across the ecliptic plane. They can reach a distance between 0.5 and 0.9 (we recall that the unit of distance of the RTBP is the Earth-Moon distance) from the ecliptic, and it seems reasonable (we recall Figure 6) that they either reach a distance close to 0.6 or to 0.8 adimensional units. In any case, note that they must spend most of their time away from the ecliptic plane and, when they cross that plane, they do it with their highest speed. Hence, we should not expect to find them very close to the triangular points.

Finally, let us mention that these regions could also be interesting for some space missions, since no control is necessary to keep an spacecraft there.

Acknowledgements

The author wants to thank interesting discussions and remarks by C. Simó. This research has been supported by the Spanish grant DGICYT PB94–0215 and the Catalan grant CIRIT 1998S0GR–00042.

References

[1] Szebehely V.: Theory of Orbits (Academic Press, 1967).

[2] Meyer K. R., Hall G. R.: Introduction to Hamiltonian Dynamical Systems and the N-Body Problem (Springer-Verlag, 1992).

[3] Giorgilli A., Delshams A., Fontich E., Galgani L., Simó C.: Effective stability for a Hamiltonian system near an elliptic equilibrium point, with an application to the Restricted Three Body Problem, *J. Differential Equations* **77** pp. 167–198 (1989).

[4] Simó C.: Estabilitat de sistemes hamiltonians, *Mem. de la Real Acad. de Ciencias y Artes de Barcelona*, Vol. XLVIII, no. 7 (1989).

[5] Celletti A., Giorgilli A.: On the stability of the Lagrangian points in the spatial Restricted Three Body Problem, *Cel. Mech.* **50** pp. 31–58 (1991).

[6] Benettin G., Fassó F., Guzzo M.: Nekhoroshev-stability of L_4 and L_5 in the spatial Restricted Three-Body Problem, *Regular and Chaotic Dynamics* (to appear).

[7] `http://ssd.jpl.nasa.gov/horizons.html`

[8] Díez C., Jorba A., Simó C.: A dynamical equivalent to the equilateral libration points of the Earth-Moon system, *Cel. Mech.* **50** pp. 13–29 (1991).

[9] Jorba À., Villanueva J.: On the Persistence of Lower Dimensional Invariant Tori under Quasi-Periodic Perturbations, *J. of Nonlinear Science* **7** pp. 427–473 (1997).

[10] Jorba À., Villanueva J.: On the Normal Behaviour of Partially Elliptic Lower Dimensional Tori of Hamiltonian Systems, *Nonlinearity* **10** pp. 783–822 (1997).

[11] Castellà E., Jorba À.: On the vertical families of two-dimensional tori near the triangular points of the Bicircular problem, *preprint* (1999).

[12] Jorba À.: A preliminary numerical study on the existence of stable motions near the triangular points of the real Earth-Moon system, *preprint* (1999).

[13] Jorba À.: Numerical computation of normal frequencies of invariant curves of higher dimensional maps, *in progress.*

[14] Gómez G., Jorba A., Masdemont J., Simó C.: Study of Poincaré Maps for Orbits near Lagrangian Points, ESOC Contract 9711/91/D/IM(SC), Final Report (1993).

[15] Simó C., Gómez G., Jorba A., Masdemont J.: The bicircular model near the triangular libration points of the RTBP, in *From Newton to Chaos*, ed. A.E. Roy and B.A. Steves, pp. 343–370 (Plenum Press, 1995).

[16] Jorba À., Villanueva J.: Numerical computation of normal forms around some periodic orbits of the Restricted Three Body Problem, *Phys. D* **114** pp. 197–229 (1998).

[17] Jorba A., Ramírez-Ros R., Villanueva J.: Effective Reducibility of Quasiperiodic Linear Equations close to Constant Coefficients, *SIAM J. on Math. Anal.* **28** pp. 178–188 (1997).

[18] Broer H., Simó C.: Hill's equation with quasi-periodic forcing: resonance tongues, instability pockets and global phenomena. *Bul. Soc. Bras. Mat.* **29** pp. 253–293 (1998).

[19] Bourgain J.: On Melnikov's persistency problem. *Math. Res. Lett.* **4** pp. 445–458 (1997).